Materials Science Forum
ISSN: 1662-9752, Vol. 893, pp 136-143
doi:10.4028/www.scientific.net/MSF.893.136

Submitted: 2016-12-22
Accepted: 2016-12-25
Online: 2017-03-27

Magnetic and Photochemical Properties of Cu Doped Hematite Nanocrystal

Myung Jong Kang, Na Hyeon An and Young Soo Kang*

Korea Center for Artificial Photosynthesis, Department of Chemistry, Sogang University, Seoul, Korea 121-742

Keywords: Photocatalyst, Hematite, Nanocrystals

Abstract. In this report, the magnetic and photochemical properties of Cu doped hematite nanocrystal was investigated intensively. The Cu doped hematite nanocrystals were prepared by hydrothermal method, changing the molar ratio of Cu precursors. The XRD and XPS techniques are used for revealing crystal and chemical state of Cu doped hematite nanocrystal. Raman spectroscopy was also used for confirming Cu atoms replacing Fe position in Cu doped hematite crystal. The UV-vis and UPS were used for assigning electronic band position for photocatalytic properties. Cu doped hematite showed the enhanced photocatalytic properties within photodegradation of methyl orange. Finally, by checking magnetic hysteresis loops of Cu doped hematites with VSM, it was revealed that the magnetic property of Cu doped hematite nanocrystal was increased after doping Cu into hematite nanocrystal, get the distortion of magnetic sub-lattices.

Introduction

Hematite (α-Fe_2O_3) have attracted much attention because of their potential applications in photocatalysts and other electronic materials based on their distinct characteristics. Hematite is widely used for lithium ion battery,[1] magnetic fluid,[2] biotechnology,[3] catalyst,[4] environmental remediation[5] and magnetic resonance image.[6] Among those application fields, photocatalytic and magnetic applications are intensively attractive fields because hematite has optimum range of band gap for solar light absorption. This band gap position allows visible range absorption, which can utilize the large amount of solar energy.[4] Furthermore, hematite is one of the abundant and low cost materials on the earth with a good chemical stability in both acidic and alkaline medium and low toxicity.[7-10] Despite the strengths of above, short electron diffusion length (2~4nm), short life times of the excited electrons and poor oxygen evolution kinetics are resulting in poor catalytic efficiency of hematite. Also, hematite has the anti-ferromagnetic characteristic with a corundum structure, of which Neel temperature is ~ 955 K and Morin transition at ~ 263 K.[11, 12] The oriented magnetic sub-lattices are along the rhombohedral [111] axis and antiparallel on them. Above T_M, the moments are slightly tilted from antiferromagnetic axis, which results in a low net magnetization along the plane.[13]

To overcome catalytic and magnetic drawbacks of hematite, doping other transition metal is one of the solutions. Recently, many transition metals such as Ti,[14] Mn,[15] Ni and Zn[16] have been doped into hematite to increase catalytic and magnetic properties. However, with the best of our knowledges, Cu doped hematite have not been investigated intensively to study photoelectrochemical and magnetic properties on it, except theoretical calculation by using first principal calculation method.[17]

Herein, we report peculiar photoelectrochemical and magnetic properties of Cu doped hematite nanocrystals which were synthesized by simple hydrothermal method. Copper (II) nitrate was used for Cu precursor during the synthesis of hematite nanocrystal. The photocatalytic property was studied by measuring photodegradation of methyl orange and magnetic property was studied by measuring magnetic hysteresis loop with VSM. X-ray diffraction, X-ray photoelectron spectroscopy and Raman spectroscopy were also used to get crystal structure and binding state of doped Cu in hematite nanocrystal.

Herein, we report peculiar photoelectrochemical and magnetic properties of Cu doped hematite nanocrystals which were synthesized by simple hydrothermal method. Copper (II) nitrate was used

for Cu precursor during the synthesis of hematite nanocrystal. The photocatalytic property was studied by measuring photodegradation of methyl orange and magnetic property was studied by measuring magnetic hysteresis loop with VSM. X-ray diffraction, X-ray photoelectron spectroscopy and Raman spectroscopy were also used to get crystal structure and binding state of doped Cu in hematite nanocrystal

Experimental

Preparation of pure hematite nanocrystal and films

Sodium hydroxide solution (0.2 M NaOH, Daejung Chemical Ltd., 10 mL) was slowly added into 0.2 M $FeCl_3$ solution (Sigma Aldrich) at room temperature and stirred for 10 min. The dark-brown solution was transferred to teflon-lined autoclave. The autoclave was heated in the oven for hydrothermal reaction to hematite at 150 ^oC for 4 h. After cooling, the precipitated hematite nanocrystal was collected by centrifuge and washed with DIW and ethanol. For fabricating the hematite films for photoelectrochemical characterization, F-doped tin oxide (FTO) coated glass was cleaned with sonication in mucasol solution and washed with deionized water (DIW). FTO glass was directly submerged into the gel-phase dark-brown reaction solution in teflon-lined autoclave inner. After hydrothermal reaction with same conditions above, the hematite film was washed by DIW and annealed at 550 ^oC for 4 h under the air. After annealing, the films were repeated as the same process again for the secondary growth of the films.

Preparation of Cu doped hematite nanocrystal and films

The same experimental method of preparing pure hematite nanocrystal and films were performed while the copper nitrate (2 and 5 mol% of Cu versus Fe concentration, C2 and C5 respectively, Sigma Aldrich) was added to the 0.2 M $FeCl_3$ solution. For fabricating Cu doped hematite film, FTO glass was placed vertically inside of the autoclave during reaction. After the reaction, the Cu doped hematite film was washed with DIW and annealed at 550 ^oC for 4 h under the air. After annealing, the films were repeated as the same process again for the secondary growth of the films.

Characterization

The crystalline structures of the hematite and Cu doped hematite film were investigated by the X-ray diffractometer (XRD, Rigaku miniFlex-II desktop) using Cu Kα radiation as X-ray source and scanned in the range of 20 - 80° at a speed of 1°min^{-1}. The morphology and coverage of the hematite and Cu doped hematite film surface were characterized by scanning electron microscope (SEM, Hitachi Horiba S-4300). Cross-sectional SEM images were measured to check film thickness. Raman spectra were measured by a liquid-nitrogen-cooled CCD (Symphony, Horiba Jobin Yvon)-equipped Raman spectrometer (TRIAX 550, Horiba Jobin Yvon) with 514.5 nm line emitting Ar^+ ion laser (Stabolite 2017, Spectra-Physics). Wavenumber was calibrated by checking the Raman peak position of Si. The laser power was kept at 50 mW for 10 sec. X-ray photoelectron spectrometer (XPS, Axis Ultima DLD) was used to examine the elemental composition and the chemical state of the elements in the samples. The photochemical characteristics of hematite and Cu doped hematite were investigated by photodegradation method with a methyl orange (MO). Calculation of band gap energy and optical absorption coefficient were done by measuring UV photoelectron spectrometer (ESCALAB 250Xi, Thermo Scientific) and UV-vis absorption spectroscopy (Agilent Cary 5000 UV-Vis-NIR). Magnetic properties of hematite and Cu doped hematite were measured by vibrating sample magnetometer (VSM, Lakeshore Cryotronics Inc., 7407) at 298 K.

Results and Discussion

The surface morphology of pure hematite (pure), 2% Cu doped hematite (C2) and 5% Cu doped hematite (C5) are investigated with scanning electron microscopy (Fig. 1a-c). The morphology of hematite films is similar even with the Cu doping into the hematite crystal lattice. The crystal structures of pure hematite and Cu doped hematite were investigated by X-ray diffraction (Fig. 1d).

Pure, C2 and C5 have the typical hematite XRD patterns which match with JPCDS card no. 33-0664. It is consistent with the conventional result that the hematite with less than 7 wt% doping of other transition metal into hematite does not change the XRD pattern.[18] The Cu doped hematite particle with C2 and C5 follows the Vegard's law, increasing of d-spacing value. It is shown with the increased 2Θ value in Fig. 1 d. The effect of Cu doping in hematite also was appeared on XPS spectra in Fig. 1(e-f). As the concentration of doped Cu increased, the binding energy of Fe 2p is shifted to higher energy direction, from 706.8 eV for pure hematite to 707.3 eV for C5 hematite via 707.0 eV for C2 hematite because of the Cu has higher binding energy compared with Fe (Fig. 1e). This trend is also shown in O 1s spectra, which is the binding energy of peak position shifted to higher binding energy region, from 525.6 eV for pure hematite to 526.1 eV for C5 hematite via 525.8 eV for C2 hematite (Fig. 1f).

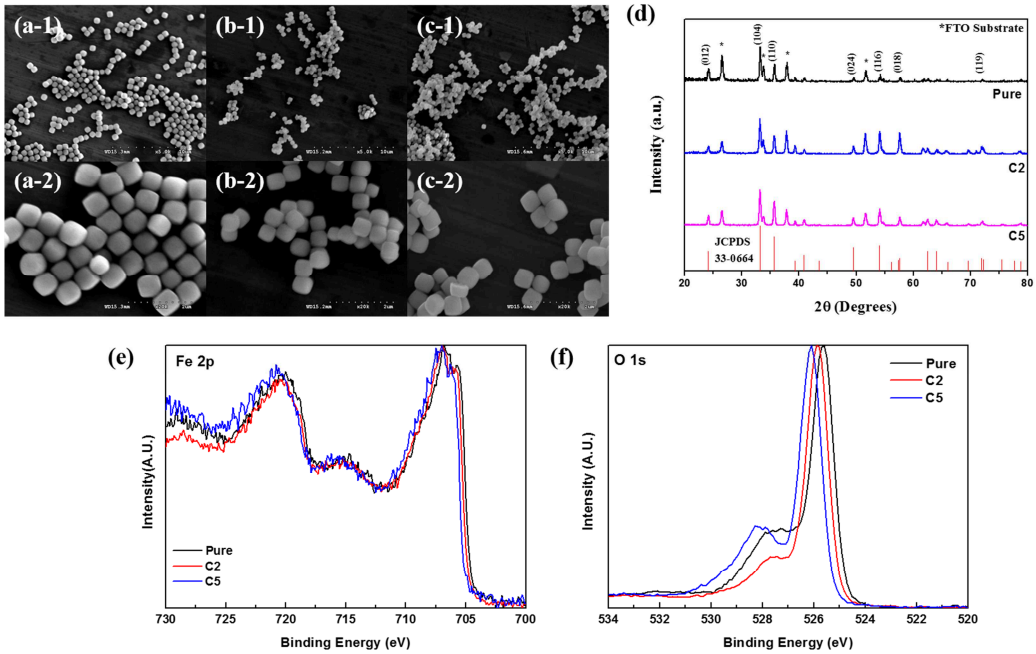

Figure 1. SEM images of pure hematite (a-1. a-2), C2 hematite (b-1, b-2) and C5 hematite (c-1, c-2), (d) X-ray diffraction patterns of pure hematite, C2 and C5 hematite thin films, XPS spectra of (e) Fe 2p and (f) O 1s of Pure hematite, C2 and C5 hematite.

The evidence for Cu doping in the position of Fe atoms by substitution is shown by Raman spectroscopy in Fig. 2. Hematite has the corundum structure and it belongs to the D_{3d} point group. Only two A_{1g} modes and five E_g modes are Raman active, while two A_{2u} modes and four E_u modes are infrared active only.[19-22] In order for a molecule to be Raman-active, there must be a change in the polarizability of the molecule while IR-active modes are induced by change in dipole moment within the molecule. The polarizability is the proportionality between the induced dipole moments and the electric field inducing it. Raman selection rule is defined as $\delta\alpha/\delta q \neq 0$ where α is the polarizability and q is displacement in the inter-nuclear distance. If the polarizability ellipsoid is changed in size or shape as a result of molecular vibration, a Raman spectrum will appear. Seven Raman-active bands were found in the range of 200-700 cm^{-1} such as A_{1g} (222, 496 cm^{-1}) and E_g (242, 291, 408, 610 cm^{-1}). [19, 20]

However, IR-active E_u mode was found at 660 cm^{-1} at C5 hematite sample in Fig. 2b. This extra peak at 660 cm^{-1} seems to be related to disorder effects.[19] E_u mode is originated from Fe-O-Fe asymmetric bending as seen in Fig. 2b. As Cu ion was doped into crystal lattice of hematite, Fe was substituted with Cu, inducing bond length change. At equilibrium, bond length of Fe-O-Fe was L and it changed to L-Q as it asymmetrically bent. Therefore, it was Raman-inactive since $\delta\alpha/\delta q=0$. With Cu doping, bond lengths of Fe-O-Cu was L-Q_1 or L-Q_2 during asymmetric bending. Cu atom doping caused $\delta\alpha/\delta q \neq 0$. In other words, the change in the polarizability ellipsoid is giving rise to E_u mode in Raman spectra. It appeared to be very weak peak at 660 cm^{-1}. The reason for this phenomenon has

been already reported as the disorder of the crystal structure which was induced by the dopants materials.

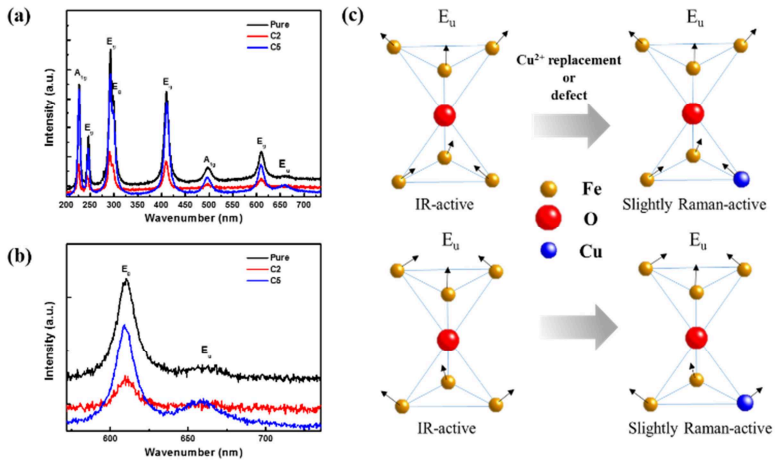

Figure 2. (a) Raman spectra of pure hematite, C2 and C5 hematite and (b) closed view at 550 – 750 nm. (c) Scheme for changing structure of from IR-active to Raman active when Cu doped in pure hematite.

The optical absorption coefficients (α) were calculated by the following eq. 1 from the optical transmittance (T) measured by UV-vis spectrometer and the film thicknesses (L) determined from cross-sectional SEM images in Fig. 3a.

$$\alpha = -\ln T(\lambda)/L \quad \text{(Eq. 1)}$$

α^{-1} corresponds to the light penetration depth.[23] The depths were determined as 90, 121 and 100 nm, respectively, for pure hematite, C2 and C5 hematite at 520 nm of incident wavelength. The deeper light travels into the films, the more photons can excite the electrons near the substrate. Tauc plots were drawn to estimate the value of optical band gap in Fig. 3b.
The value of band gap was determined by drawing a dotted intra-polated line and finding a point where dotted line crosses x-axis. The band gap energy was calculated by following eq 2.

$$E_g = 1240/\lambda \text{ (eV)} \quad \text{(Eq. 2).}$$

The calculated band gap values of hematite were obtained as 2.03, 2.09 and 2.08 eV, respectively, with pure, C2 and C5 hematite. These values are consistent with the well-known band gap energy of hematite (2.0 – 2.2 eV).[24] Doping Cu into pure hematite thin film slightly increases band gap energy. Valence band position of hematite, HOMO energy level in high vacuum, was determined by using UPS in Fig. 3(c-e).[25] Valence band energies in high vacuum were determined as -6.83, -8.08, and -7.98 eV, respectively for pure, C2 and C5 hematite. Finally, band gap diagram was drawn by considering the calculated band gap energy from UV-Vis spectra and valence band position from UPS data in Fig. 3f. Conduction band position was determined by following eq. 3.

$$\text{Valance band energy } (E_{VB}) = \text{Conduction band energy } (E_{CB}) - E_g. \quad \text{(Eq. 3)}$$

With Cu doped hematite, valence band position was lowered while no significant difference in band gap appeared. As it has been reported in the previous report, the potential of oxygen evolution is in between the valence and conduction band of hematite crystals.[9,18] When photons are absorbed by hematite, electrons are excited and holes are produced in the valence band. Holes will oxidize water and generate oxygen gas. As valence band energy level becomes lower, the gap between valence band and water oxidation potential increases, which makes it hard to transfer holes from valence band into oxidation potential level.

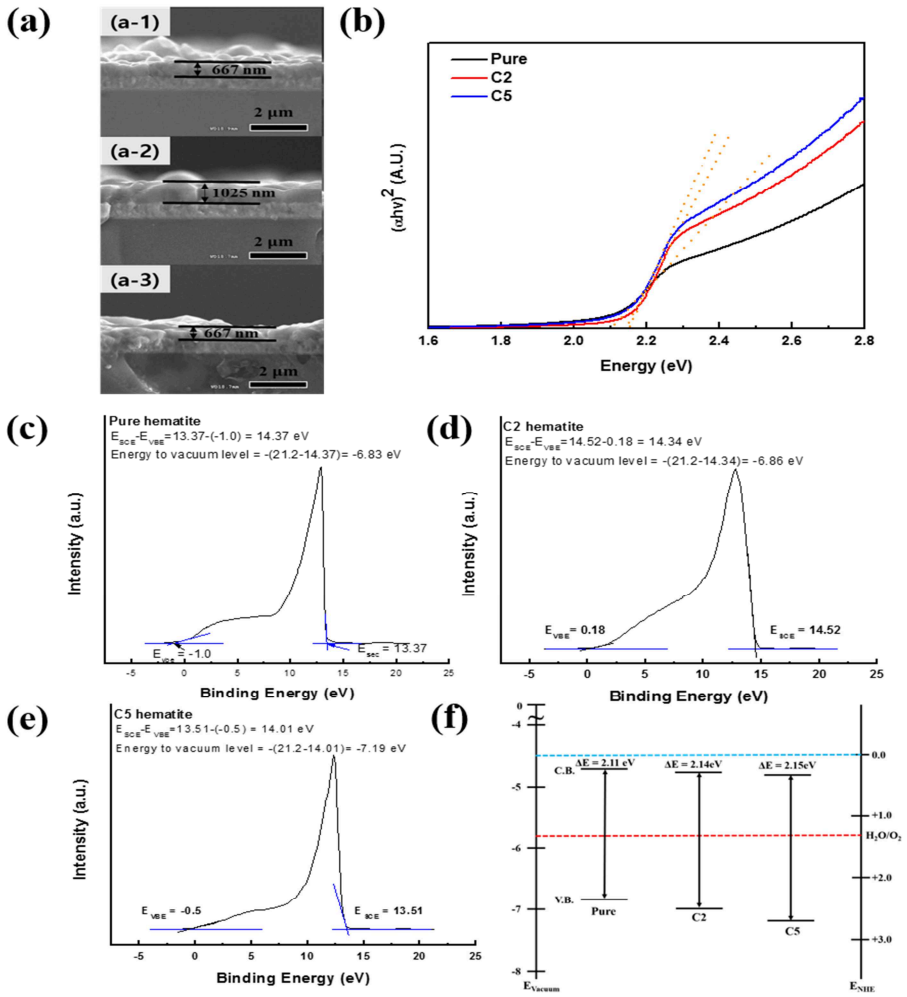

Figure 3. (a) Cross-sectional SEM images of (a-1) pure hematite (a-2) C2 hematite and (a-3) C5 hematite thin films. (b) Tauc plots of pure hematite, C2 and C5 hematite. The band gap energy of pure hematite, C2 and C5 hematite taken from the points where the slope and baseline meet, indicating 2.11, 2.14, 2.15 eV, respectively. (c-e) UPS spectra of (c) pure, (d) C2 and (e) C5 hematite thin films. EVBE and ESCE indicate valence band energy and secondary cutoff energy, respectively and (f) Band gap diagrams of pure and Cu-doped hematite films determined from UV-vis absorbance spectra and UPS measurements.

The photocatalytic activity of Cu doped hematite was investigated by photodegradation of methyl orange (MO) dye in Fig. 4 (a). The photodegradation of MO dye occurs on the surface of Cu doped hematite nanocrystals. The decrease in absorption intensity of MO solution as following the photo-irradiation time is shown in Fig. 4 (b). The degradation of MO shows that prepared Cu doped hematite nanocrystals have the enhanced photocatalytic activity. The photodegradation of MO and the photocatalytic reaction follow the first order kinetics, which described by followed eq. 4.

$$-\mathrm{Ln}(C/C_o) = kt \quad \text{(Eq. 4)}$$

Where C is actual concentration of MO, C_o is initial concentration of MO and k is the photodegradation rate constant. The calculated rate constants of pure and Cu doped hematite nanocrystals within the presence of different doping ratio are shown in Fig. 4 (c). The degradation of MO is occurred by the hydroxyl radicals (•OH) and superoxide radical anions ($\bullet O^{2-}$) which are generated by the electrons in conduction band and holes in valance band, respectively, followed by the result of electron-hole separation by the irradiation of light to the hematite nanocrystals. The whole process of photodegradation of MO are summarized in the following equation 5-9.[15]

$$\text{Hematite} + h\nu \rightarrow e_{cb-} + h_{vb+} \quad \text{(Eq. 5)}$$

$$O_2 + e_{cb-} \rightarrow \bullet O^{2-} \quad \text{(Eq. 6)}$$

$$H_2O + h_{vb+} \rightarrow \bullet OH + H^+ \quad \text{(Eq. 7)}$$

$$MO + h\nu \rightarrow MO^* \quad \text{(Eq. 8)}$$

$$MO^* + \text{hematite} \rightarrow MO^+ \text{ (colorless)} + \text{hematite}\bullet \text{ (e-)} \quad \text{(Eq. 9)}$$

The degradation of MO was initiated by the formation of hydroxyl radicals and superoxide radical anions. These radical species attack the photo-excited MO molecules (MO*) and would result in the formation of MO^+ species, which are colorless species.

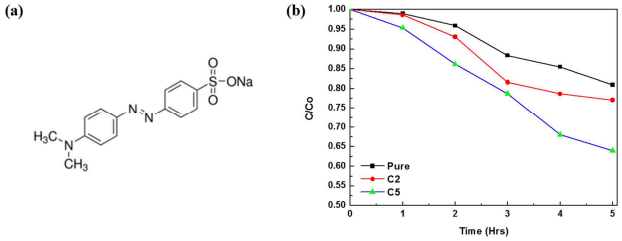

(c)

Sample	K (h^{-1})
Pure hematite	0.0423
C2 hematite	0.0521
C5 hematite	0.0893

Figure 4. (a) Molecular structure of methyl orange (MO). (b) photodegradation curve for pure, C2 and C5 hematite (c) table of k value for pure, C2 and C5 hematite.

The magnetic properties of pure and Cu doped hematite nanocrystals were studied by measuring magnetic hysteresis loop with vibrating sample magnetometer (VSM) in Fig. 5. The VSM curves for pure hematite, C2 hematite and C5 hematite are shown in Fig. 5 (a), (b) and (c), respectively. The $(BH)_{max}$ values of pure hematite, C2 hematite and C5 hematite are shown as a Table in Fig. 5 (d). The pure hematite showed the $(BH)_{max}$ as 75.472 GOe and it increased to 277.50 GOe of C2 hematite, and finally reached to 320.35 GOe of C5 hematite. The increased $(BH)_{max}$ values of hematite as increasing Cu doping ratio can be explained with the doped crystal structure as shown in Fig. 5 (e). As hematite has the oriented magnetic sub-lattices along the rhombohedral [111] axis and antiparallel on them in theoretically, it has the antiferromagnetic properties.[13]

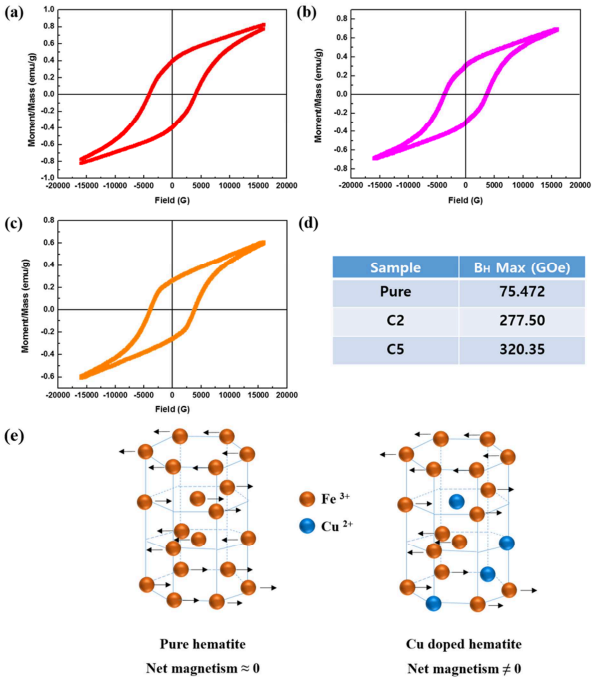

Sample	B_H Max (GOe)
Pure	75.472
C2	277.50
C5	320.35

Figure 5. VSM data of (a) pure hematite, (b) C2 hematite, (c) C5 hematite and (d) table of B_H max value depending on the doped ratio of Cu in hematite. (e) Schematic drawings for magnetic sub-lattice of pure hematite and Cu doped hematite.

Summary

In summary, doping other transition metals such as Ti, Mn and Si into the hematite was already studied intensively to increase photocatalytic or magnetic properties of hematite. However, in case of Cu, the applications of Cu doped hematite have not been studied well. The present work reports a comparison between pure hematite nanocrystal and Cu doped hematite nanocrystals synthesized by facile hydrothermal method. From this study, the Cu doped hematite nanocrystal shows the enhanced photocatalytic property in a degradation of pollutants in water (methyl orange) due to lower valence band energy position and enhanced magnetic properties of an increased $(BH)_{max}$ value due to the distortion of magnetic sub-lattices caused by doped Cu atoms. Through this work, we introduced a new insight for application of transition metal doped hematite nanocrystal for the enhanced properties of photocatalysts and magnetic materials.

References

[1] C. Wu, P. Yin, X. Zhu, C. OuYang and Y. Xie, *The Journal of Physical Chemistry B*, 2006, **110**, 17806-17812.

[2] S. Chikazumi, S. Taketomi, M. Ukita, M. Mizukami, H. Miyajima, M. Setogawa and Y. Kurihara, *Journal of Magnetism and Magnetic Materials*, 1987, **65**, 245-251.

[3] R. N. Grass, E. K. Athanassiou and W. J. Stark, *Angewandte Chemie International Edition*, 2007, **46**, 4909-4912.

[4] K. Sivula, F. Le Formal and M. Grätzel, *ChemSusChem*, 2011, **4**, 432-449.

[5] D. W. Elliott and W.-x. Zhang, *Environmental Science & Technology*, 2001, **35**, 4922-4926.

[6] S. Mornet, S. Vasseur, F. Grasset, P. Veverka, G. Goglio, A. Demourgues, J. Portier, E. Pollert and E. Duguet, *Progress in Solid State Chemistry*, 2006, **34**, 237-247.

[7] S. U. M. Khan and J. Akikusa, *The Journal of Physical Chemistry B*, 1999, **103**, 7184-7189.

[8] F. L. Souza, K. P. Lopes, E. Longo and E. R. Leite, *Physical Chemistry Chemical Physics*, 2009, **11**, 1215-1219.

[9] D. K. Zhong, J. Sun, H. Inumaru and D. R. Gamelin, *Journal of the American Chemical Society*, 2009, **131**, 6086-6087.

[10] K. Kamada, T. Hyodo and Y. Shimizu, *The Journal of Physical Chemistry C*, 2010, **114**, 3707-3711.

[11] D. Schroeer and R. C. Nininger, *Physical Review Letters*, 1967, **19**, 632-634.

[12] R. C. Nininger and D. Schroeer, *Journal of Physics and Chemistry of Solids*, 1978, **39**, 137-144.

[13] N. Amin and S. Arajs, *Physical Review B*, 1987, **35**, 4810-4811.

[14] P. Zhang, A. Kleiman-Shwarsctein, Y.-S. Hu, J. Lefton, S. Sharma, A. J. Forman and E. McFarland, *Energy & Environmental Science*, 2011, **4**, 1020-1028.

[15] H. G. Cha, H. S. Noh, M. J. Kang and Y. S. Kang, *New Journal of Chemistry*, 2013, **37**, 4004-4009.

[16] C. A. Barrero, J. Arpe, E. Sileo, L. C. Sánchez, R. Zysler and C. Saragovi, *Physica B: Condensed Matter*, 2004, **354**, 27-34.

[17] X. Y. Meng, G. W. Qin, S. Li, X. H. Wen, Y. P. Ren, W. L. Pei and L. Zuo, *Applied Physics Letters*, 2011, **98**, 112104.

[18] H. G. Cha, J. Song, H. S. Kim, W. Shin, K. B. Yoon and Y. S. Kang, *Chemical Communications*, 2011, **47**, 2441-2443.

[19] D. Varshney and A. Yogi, *Journal of Advanced Ceramics*, 2014, **3**, 269-277.

[20] A. Zoppi, C. Lofrumento, E. M. Castellucci, C. Dejoie and P. Sciau, *Journal of Raman Spectroscopy*, 2006, **37**, 1131-1138.

[21] I. Chamritski and G. Burns, *The Journal of Physical Chemistry B*, 2005, **109**, 4965-4968.

[22] M. V. Abrashev, A. P. Litvinchuk, M. N. Iliev, R. L. Meng, V. N. Popov, V. G. Ivanov, R. A. Chakalov and C. Thomsen, *Physical Review B*, 1999, **59**, 4146-4153.

[23] I. Cesar, K. Sivula, A. Kay, R. Zboril and M. Grätzel, *The Journal of Physical Chemistry C*, 2009, **113**, 772-782.

[24] A. Duret and M. Grätzel, *The Journal of Physical Chemistry B*, 2005, **109**, 17184-17191.

[25] W.-J. Chun, A. Ishikawa, H. Fujisawa, T. Takata, J. N. Kondo, M. Hara, M. Kawai, Y. Matsumoto and K. Domen, *The Journal of Physical Chemistry B*, 2003, **107**, 1798-1803.